	D10	D10/IL-2Rβ/γc
Data collection		
Space group	P1	P1
Cell dimensions		
a,b,c (Å)	55.873, 75.019, 76.812	118.226, 118.099, 236.115
α, β, Y (°)	101.458, 102.287, 104.313	99.855, 99.862, 99.735
Wavelength (Å)	1Å	0.97Å
Resolution (Å)	50.00-3.10(3.21-3.10)*	52.20-3.80(3.93-3.80)*
R_{merge} (%)	5.6 (44.0)	12.5 (42.8)
<I/σI>	14.5 (2.0)	6.7 (2.1)
Completeness (%)	99.0 (98.4)	99.0 (98.7)
Unique reflections	20383	111101
Redundancy	2.2 (2.2)	2.1 (2.2)
Refinement		
Resolution (Å)	49.2-3.1	52.2-3.8
No. reflection work/test	19,304/996	109247/1854
R_{cryst}/R_{free} (%)	22.1/26.3	29.3/34.2
Avg. B-values (Å^2)	84.6	99.9
R.m.s deviations		
Bond lengths (Å)	0.009	0.006
Bond angles (°)	1.02	1.09
Ramachandran plot (%)		
Favored/ allowed/ outliers	98/1.9/0.1	93.4/6.4/0.2

Supplementary Table 1. Crystallographic statistics of D10 and the D10/IL-2Rβ/γc complex.

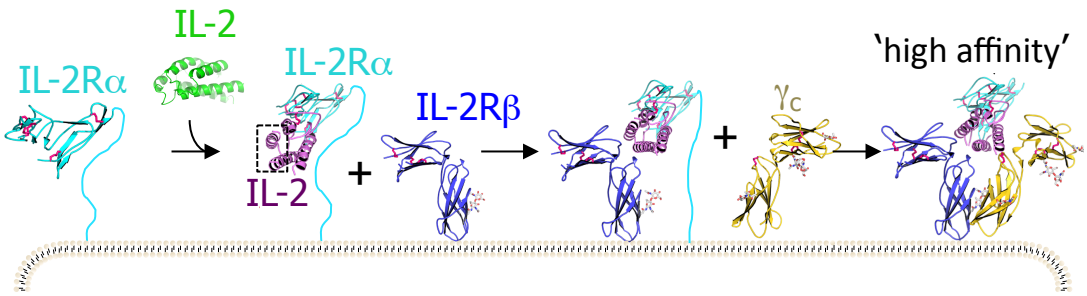

Supplementary Figure 1. Structural basis for assembly of the IL-2 quaternary complex in which IL-2 engages IL-2Rα, and is then presented to IL-2Rβ, followed by engagement of γ_c (adapted from ref. 11). Boxed region of IL-2 bound to CD25 is the IL-2Rβ binding site (upper helix C and lower helix A).

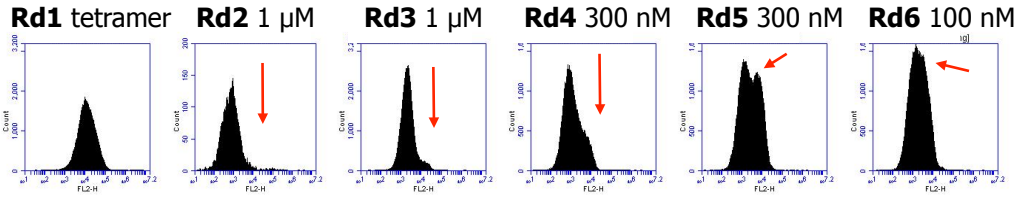

Supplementary Figure 2. Flow cytometric analysis of first generation IL-2 error-prone yeast library selections. Progressively lower concentrations of IL-2Rβ were used in each round. Sequencing of round 6 clones revealed an enrichment for clones containing a L85V substitution, which formed the basis of a second generation core library around this position (see Fig. 1b). Red arrows indicate enriching population of tetramer positive yeast clones.

												Affinity for IL-2Rβ		
residue #	*24*	*65*	**74**	*76*	**80**	**81**	**85**	**86**	**89**	**92**	**93**	**K_d(nM)**	**k_{on}(1/ms)**	**k_{off}(1/s)**
wt IL-2	*I*	*P*	**Q**	*K*	**L**	**R**	**L**	**I**	**I**	**I**	**V**	280	$7.9x10^5$	0.22
5-1			R									235	$3.1x10^5$	0.073
5-2							V					77	$5.8x10^5$	0.045
6-6						I	V					49	$1.2x10^6$	0.061
A2			H			T	V	V		F	I			
B1			N		F	D	V	V	V	F		1.6	$3.1x10^6$	0.005
B11	*V*		S		F	D	V	V		F				
C5		*H*	N		V	T	V	V		F		10	$1.6x10^6$	0.016
D10			H		F	D	V	V		F		1.3	$4.1x10^6$	0.0051
E10			S		F	D	V	V		F		1.3	$4.3x10^6$	0.0055
G8			N	*I*	F	D	V	V		F		1.5	$3.2x10^6$	0.0049
H4			S			T	V			F		14	$9.4x10^5$	0.013
H9					F	D	V	V		F		1.4	$4.1x10^6$	0.0056
CONSENSUS					F	D	V	V		F				

Supplementary Figure 3. Mutations in first and second generation superkines. Initial discovery of the L85V core mutation from an error-prone library (variants 5-2, 6-6) led to a second generation site-directed IL-2 library targeting hydrophobic core residues indicated. A consensus sequence of L80F/R81D/L85V/I86V/I92F emerged among the highest affinity superkines. Numbering scheme for super-2 variants is on left column. Gray highlighting and italics indicates mutations that arose outside of the targeted codons. Affinities and kinetic rate constants (right columns) were determined by surface plasmon resonance, raw data and curve fits shown in Supplementary Fig. 5.

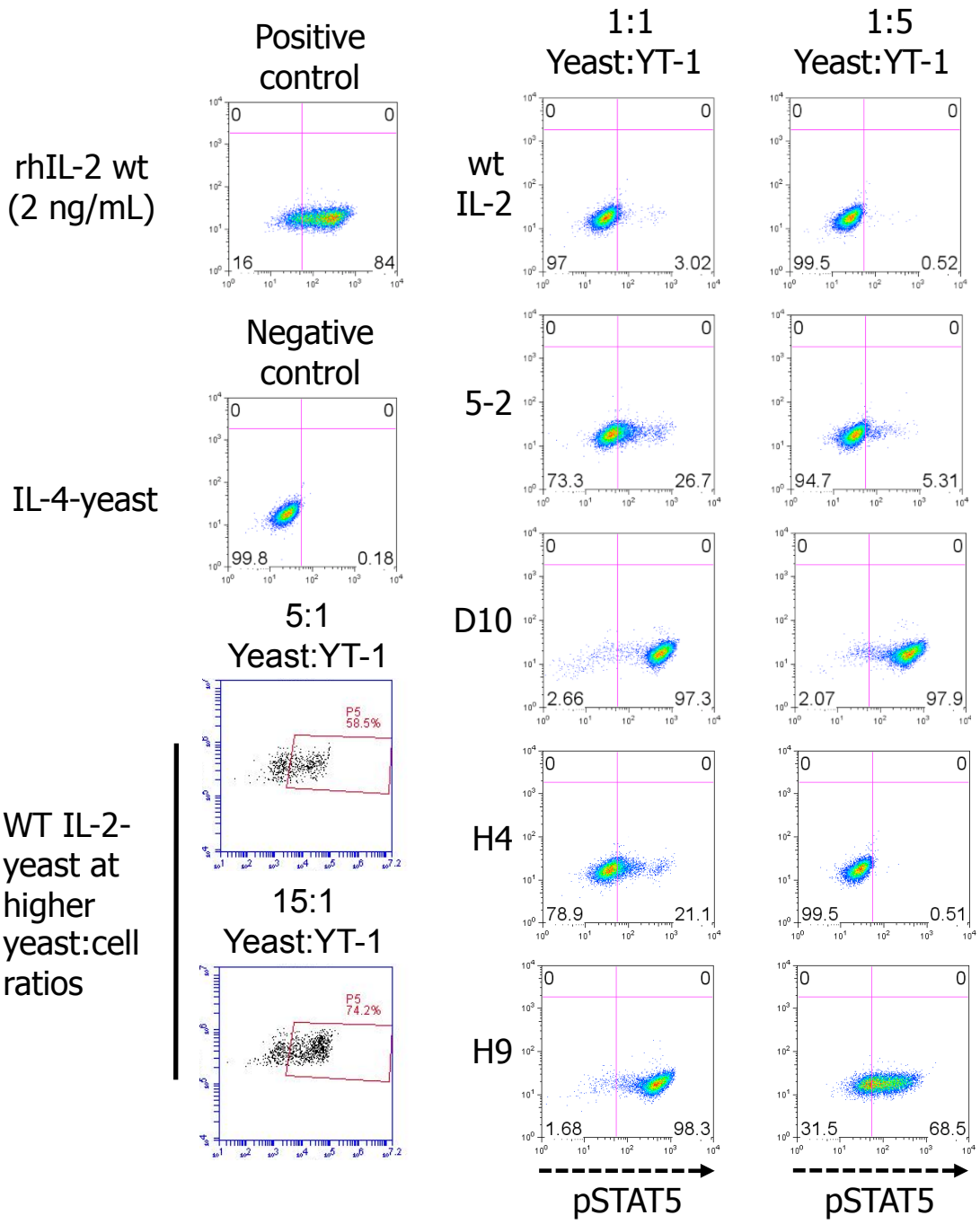

Supplementary Figure 4. On-yeast phosphorylation of STAT5 (pSTAT5) on YT-1 NK cells analyzed by flow cytometry at multiple yeast to cell ratios. The positive control for pSTAT5 induction was recombinant human IL-2. The negative control used was yeast displaying IL-4, which induces pSTAT6 and whose receptor is absent in YT-1 cells (see Supplementary Fig. 9a).

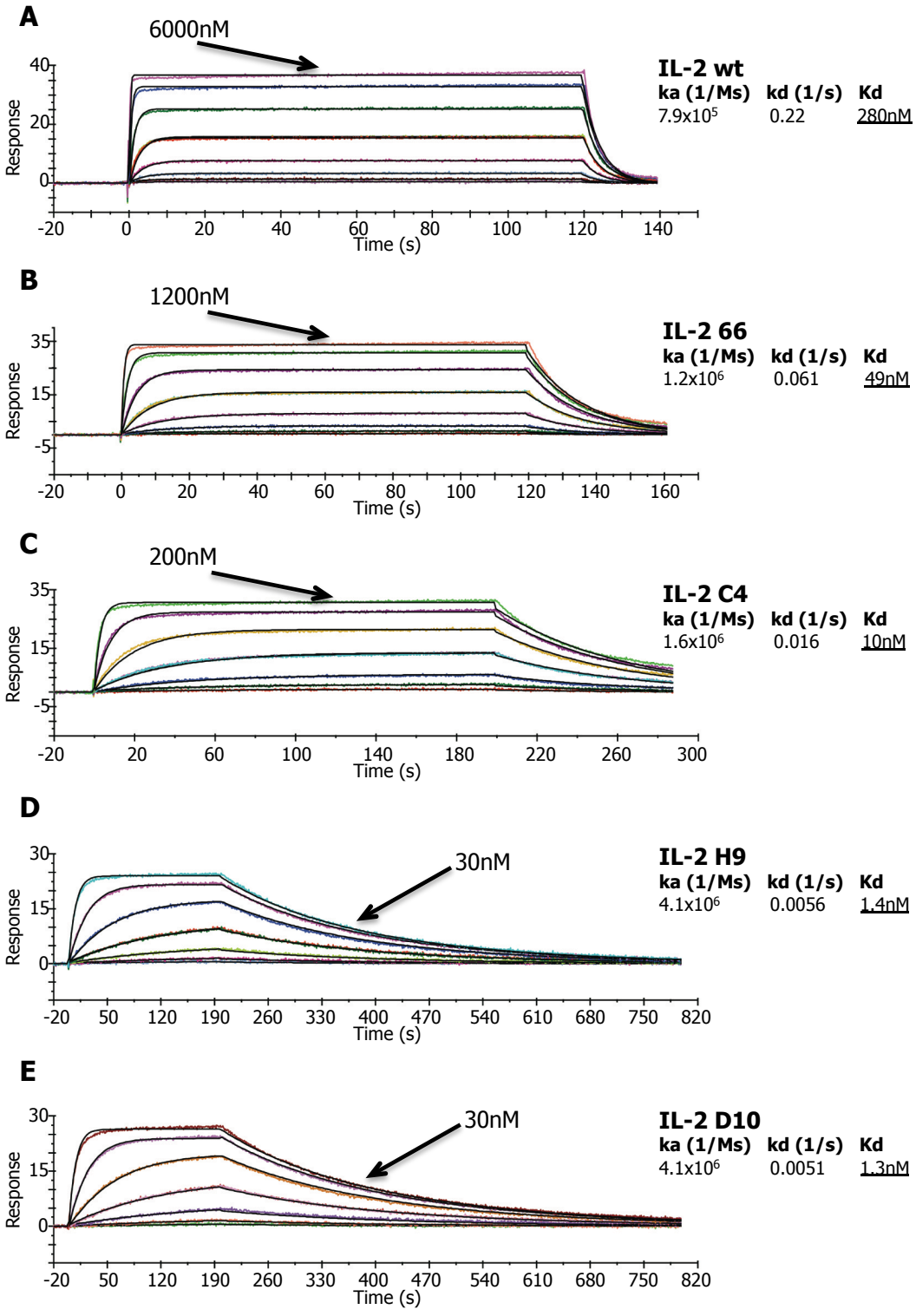

Supplementary Figure 5. Surface plasmon resonance analysis of IL-2 and super-2 variants binding to IL-2Rβ.

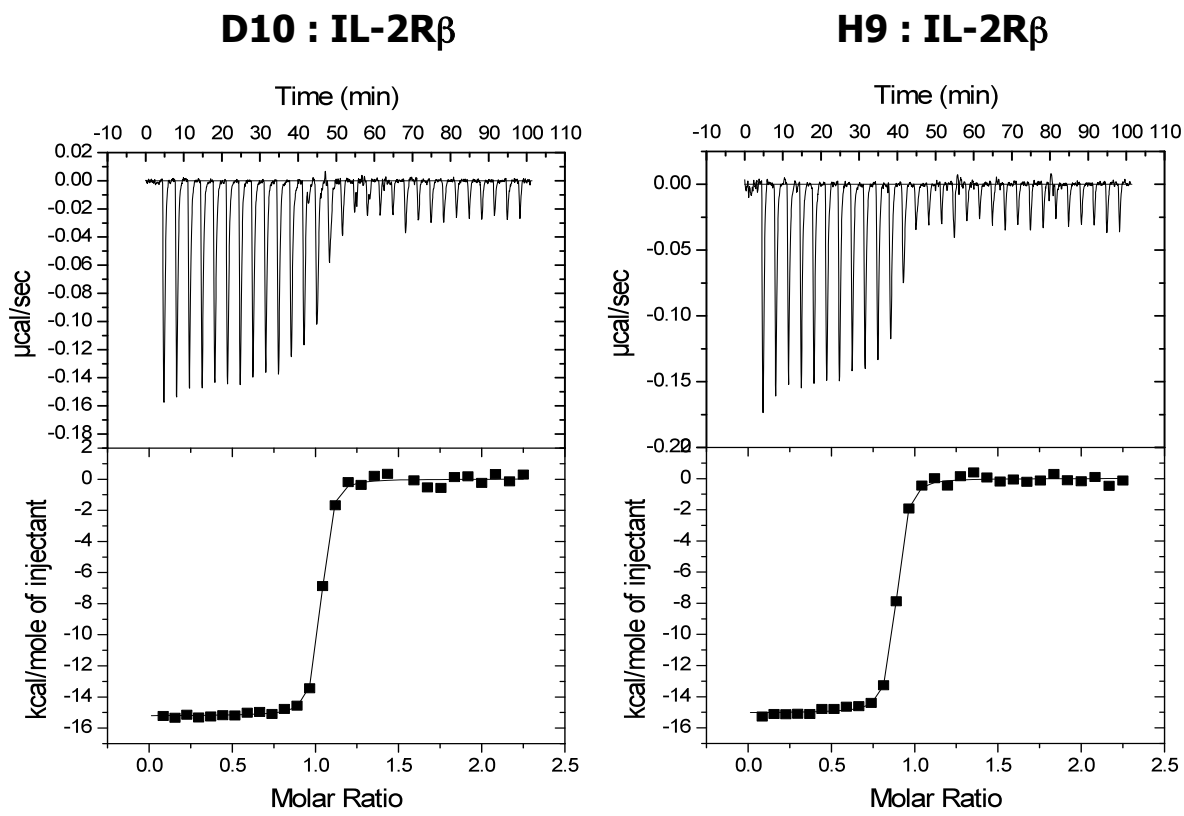

	IL-2*	IL-2 / CD25*	D10	H9
K_D (nM)	144	63	2.15	2.92
ΔH (kcal/mol)	-7.64	-6.92	-15.2	-15.0
ΔS (cal/mol-K)	4.79	8.95	-13.1	-13.1
N	1.11	0.64	1.00	0.856
T (K)	288	288	288	288

* From Rickert et al., 2004.

Supplementary Figure 6. Isothermal Titration Calorimetry of IL-2 and super-2 variants binding to IL-2Rβ.

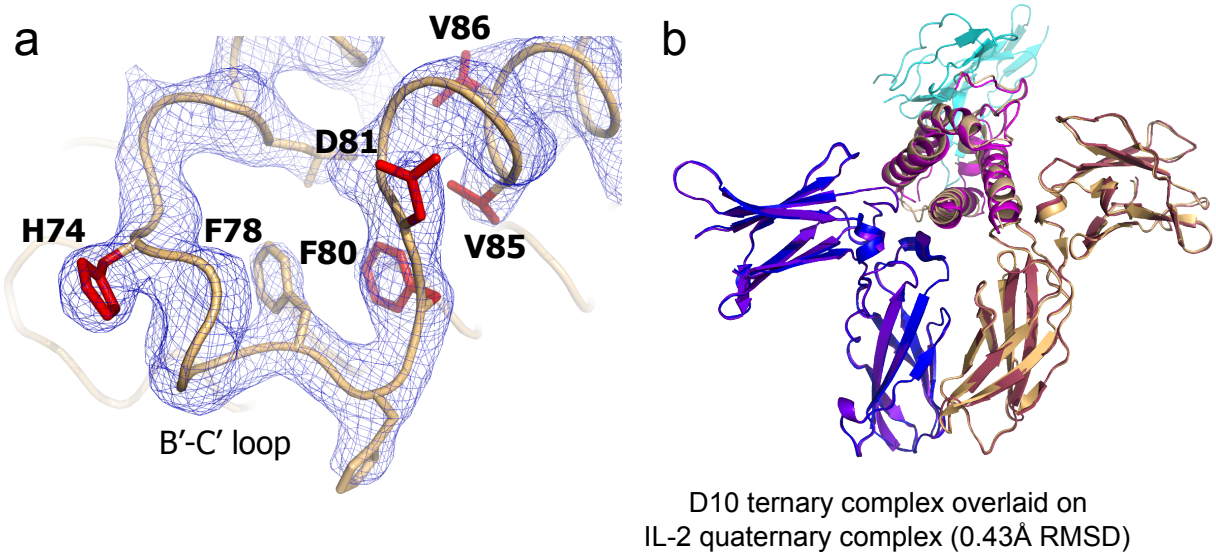

Supplementary Figure 7. Electron density and structural alignment of D10 superkine. **a**, $2mF_o$-DF_c simulated-annealing composite-omit map of B'-C' loop of unliganded D10 at 1.5 σ contour level. **b**, Structural alignment of D10, IL-2Rβ/γ_c ternary complex and WT IL-2/IL-2Rβ/γ_c/CD25 quaternary complex (2B5I) reveals that D10 heterodimerizes IL-2Rβ/γ_c with the same geometry as WT IL-2.

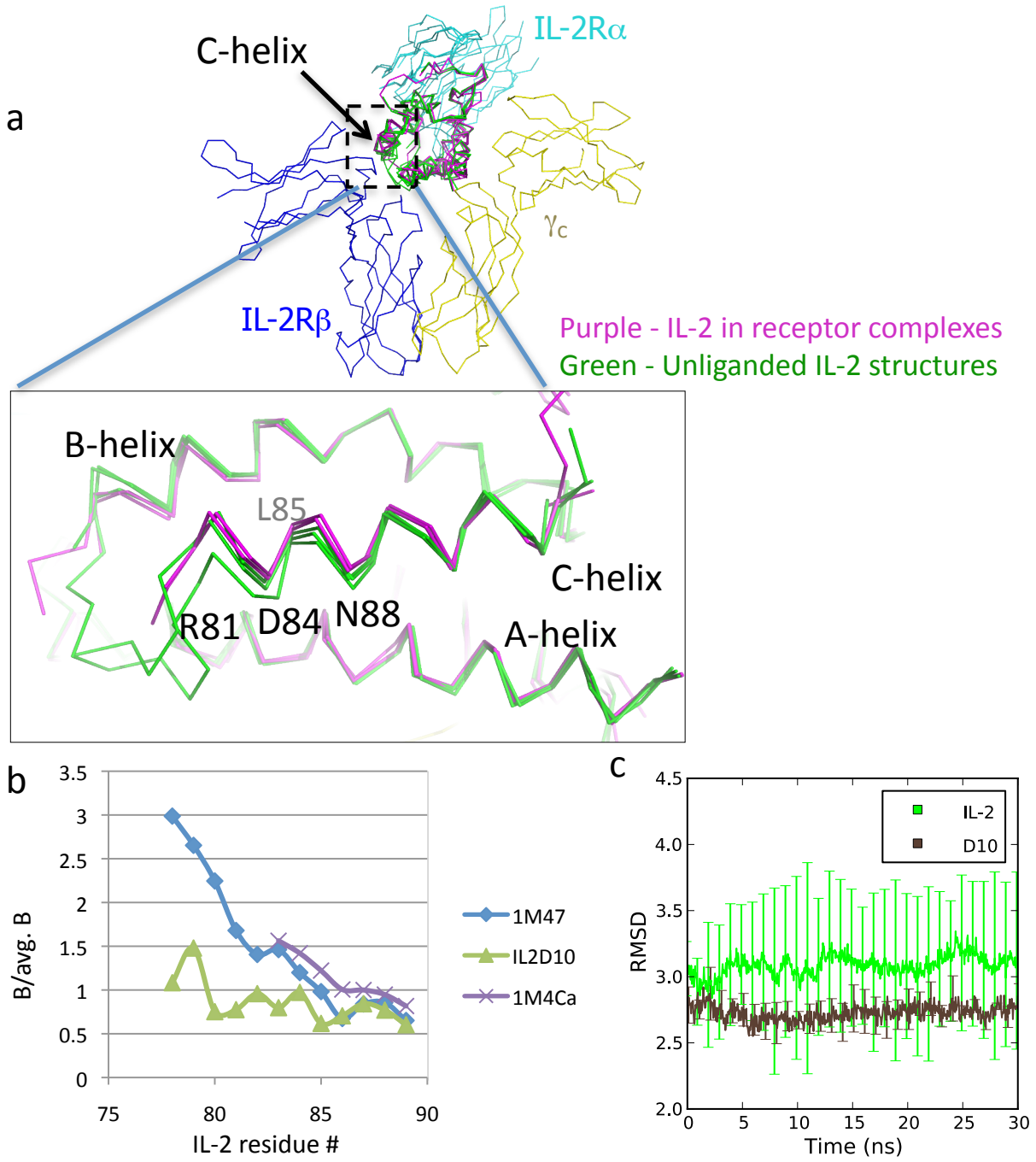

Supplementary Figure 8. Conformational variability in IL-2 C-helix. **a**, Crystal structures of three unliganded IL-2 molecules (PDBID: 3INK, 1RMC, 1M4C) in green, and two IL-2 receptor complexes in purple (PDBID: 1Z92, 2B5I). Three residues that hydrogen bond with IL-2Rβ are indicated on the outer face of helix C (R81, D84, N88), as is the position of the first generation super-2 founder mutation (L85). **b**, Elevated crystallographic B-factors in helix C relative to the other portions of the molecule. The 1M4C IL-2 structure is disordered in the B-C loop and part of helix C. **c**, MD simulation of D10 and with IL-2 starting in a receptor-bound like conformation, and monitoring the divergence (RMSD) of the B-C loop and helix C from the actual receptor-bound conformation. IL-2 rapidly "wanders" from the receptor-like conformation and experiences drastic fluctuations compared to D10. Error bars in **c** are the standard deviation of the RMSD at a given time-point from all the simulations.

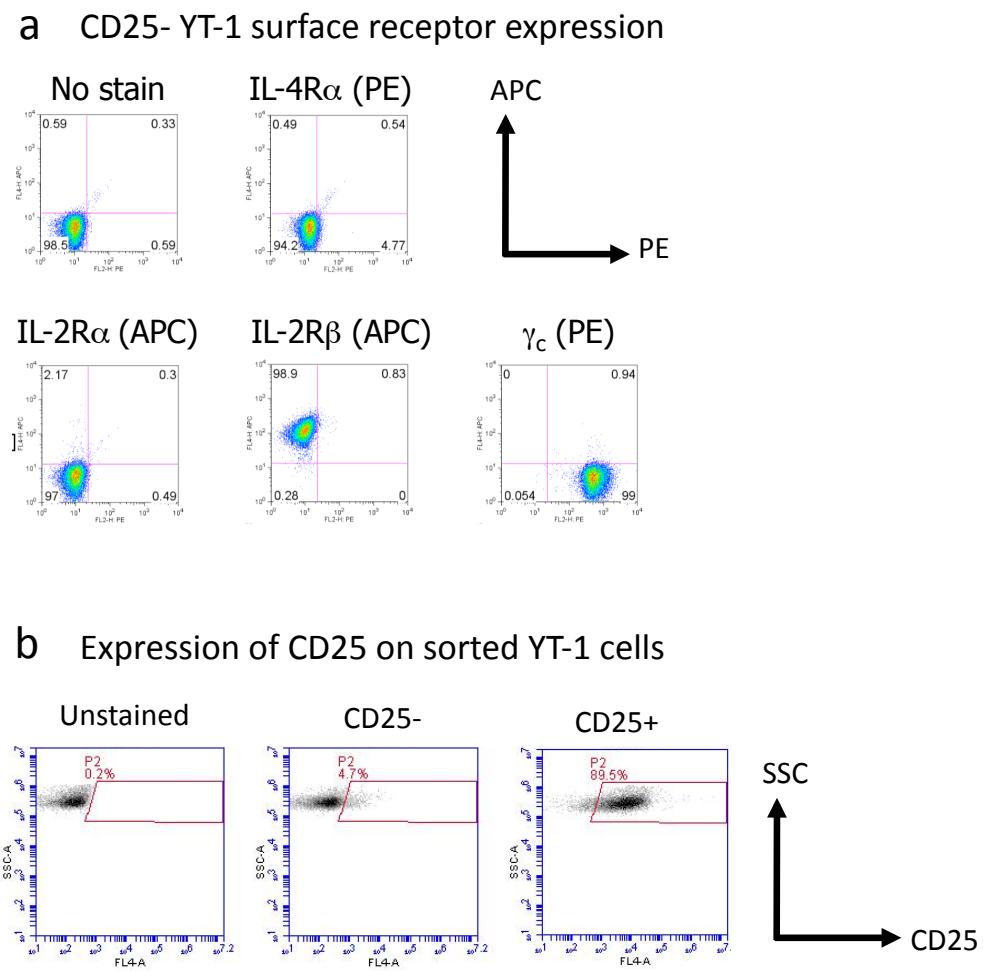

Supplementary Figure 9. **a**, Flow cytometry analysis of receptor expression in CD25$^-$ YT-1 cells. YT-1 cells were labeled to detect the presence of IL-2Rα, IL-2Rβ, γ_c, and IL-4Rα. IL-2Rβ and γ_c were readily detected, but staining for IL-2Rα and IL-4Rα was equivalent to background. For the CD25$^+$ YT-1 cells used in Fig. 3, CD25$^+$ YT-1 cells were purified using anti-CD25 magnetic beads. **b**, CD25 expression on purified CD25$^-$ and CD25$^+$ YT-1 cell subsets following magnetic cell sorting.

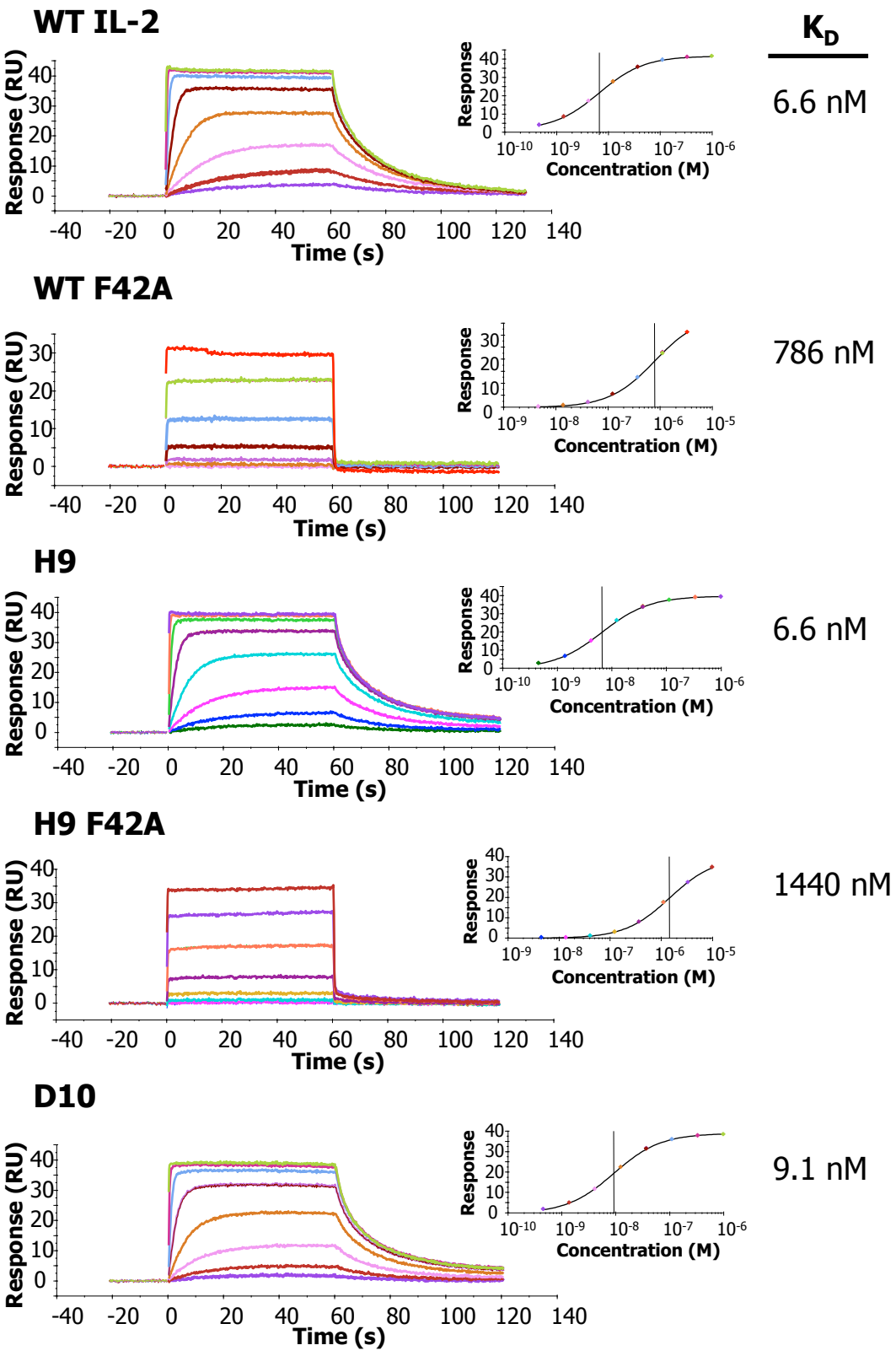

Supplementary Figure 10. Surface plasmon resonance analysis of IL-2 and super-2 variants binding to CD25.

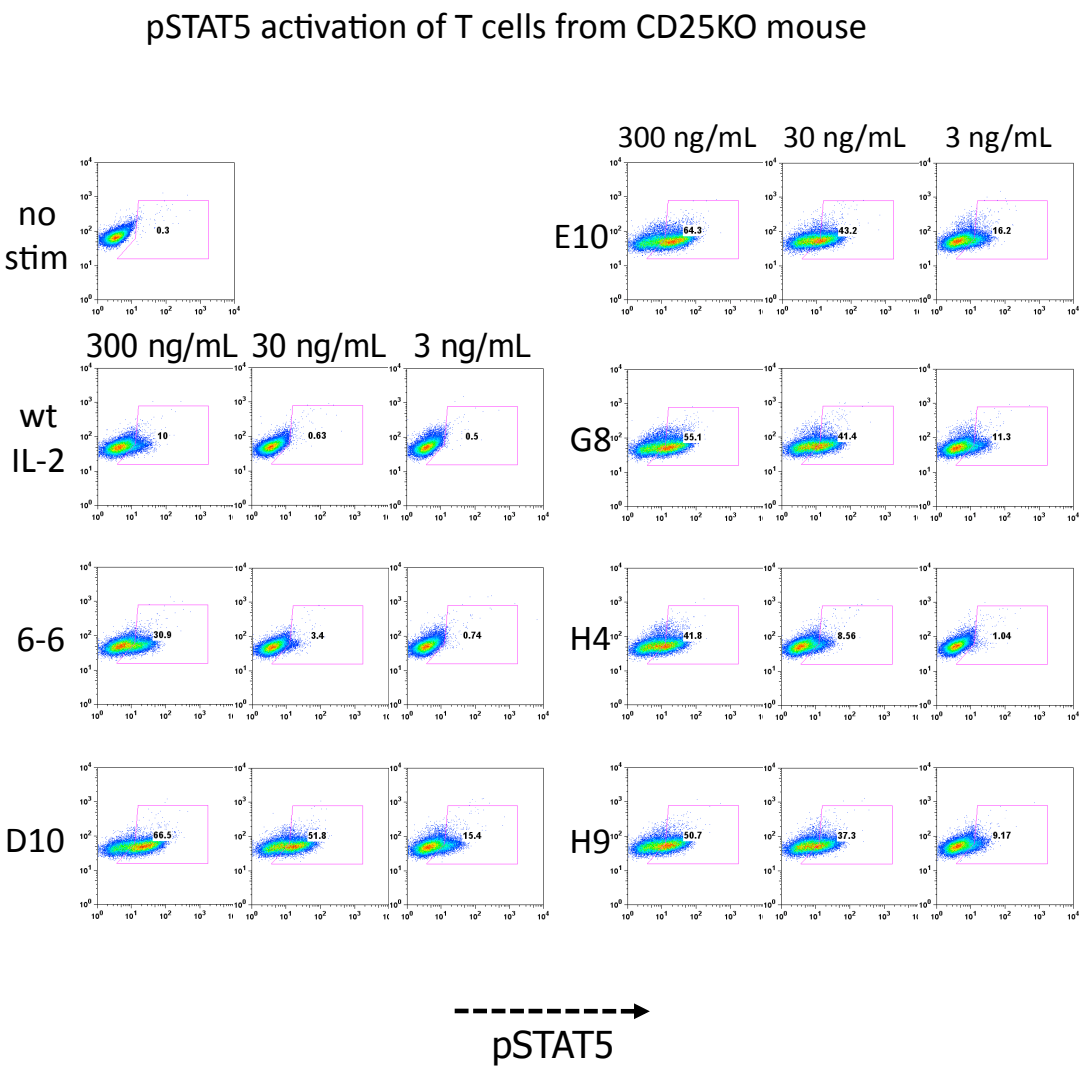

Supplementary Figure 11. STAT5 phosphorylation (pSTAT5) in T cells isolated from $CD25^{-/-}$ mice. Additional titration points were used to calculate EC_{50} values that are not shown here.

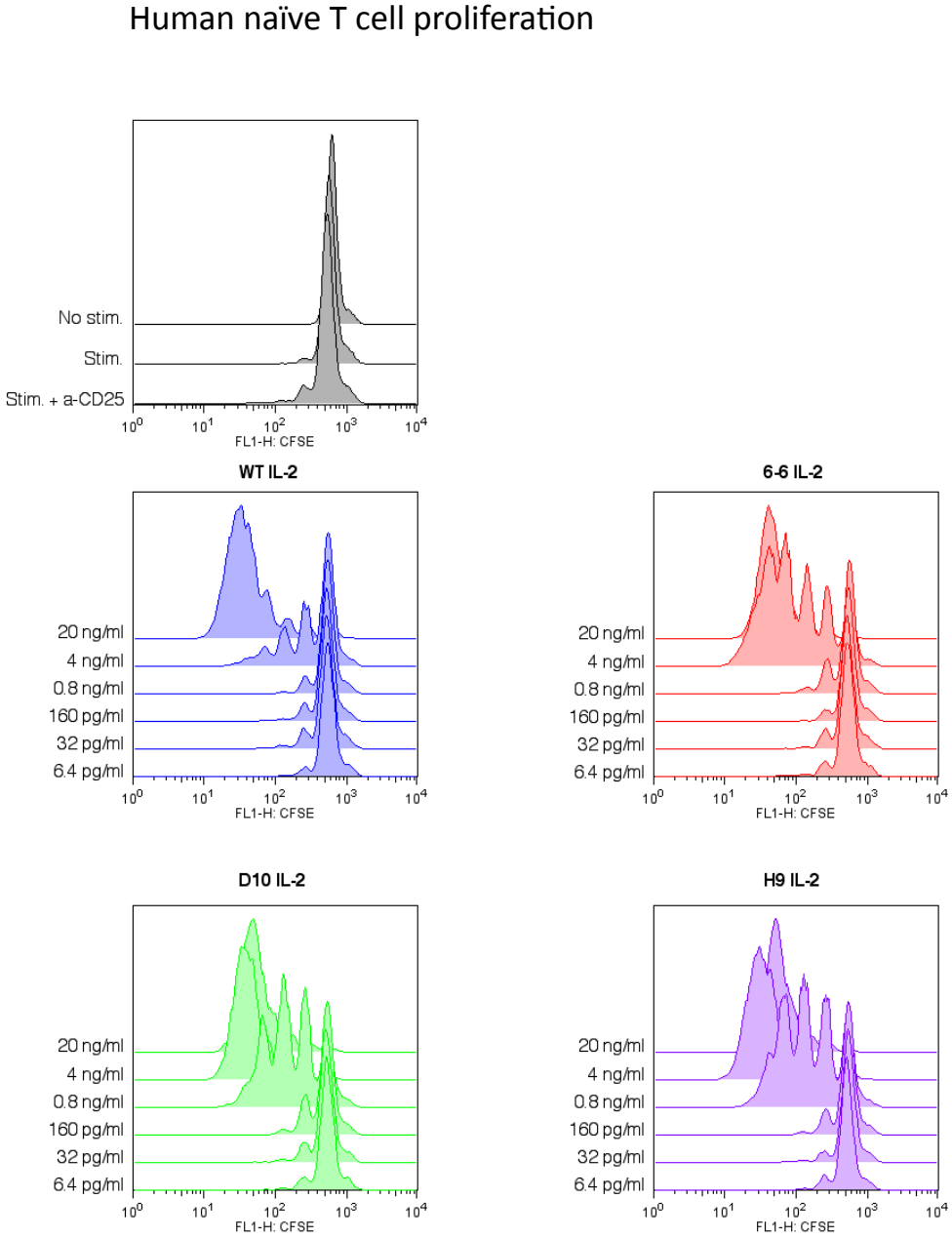

Supplementary Figure 12. Individual IL-2 and super-2 dose-response titrations measuring naïve T cell proliferation by CFSE staining. EC_{50} values were derived from these titrations. Top panel represents negative control showing that neither anti-CD3 nor anti-CD25 antibody induced proliferation in the absence of IL-2.

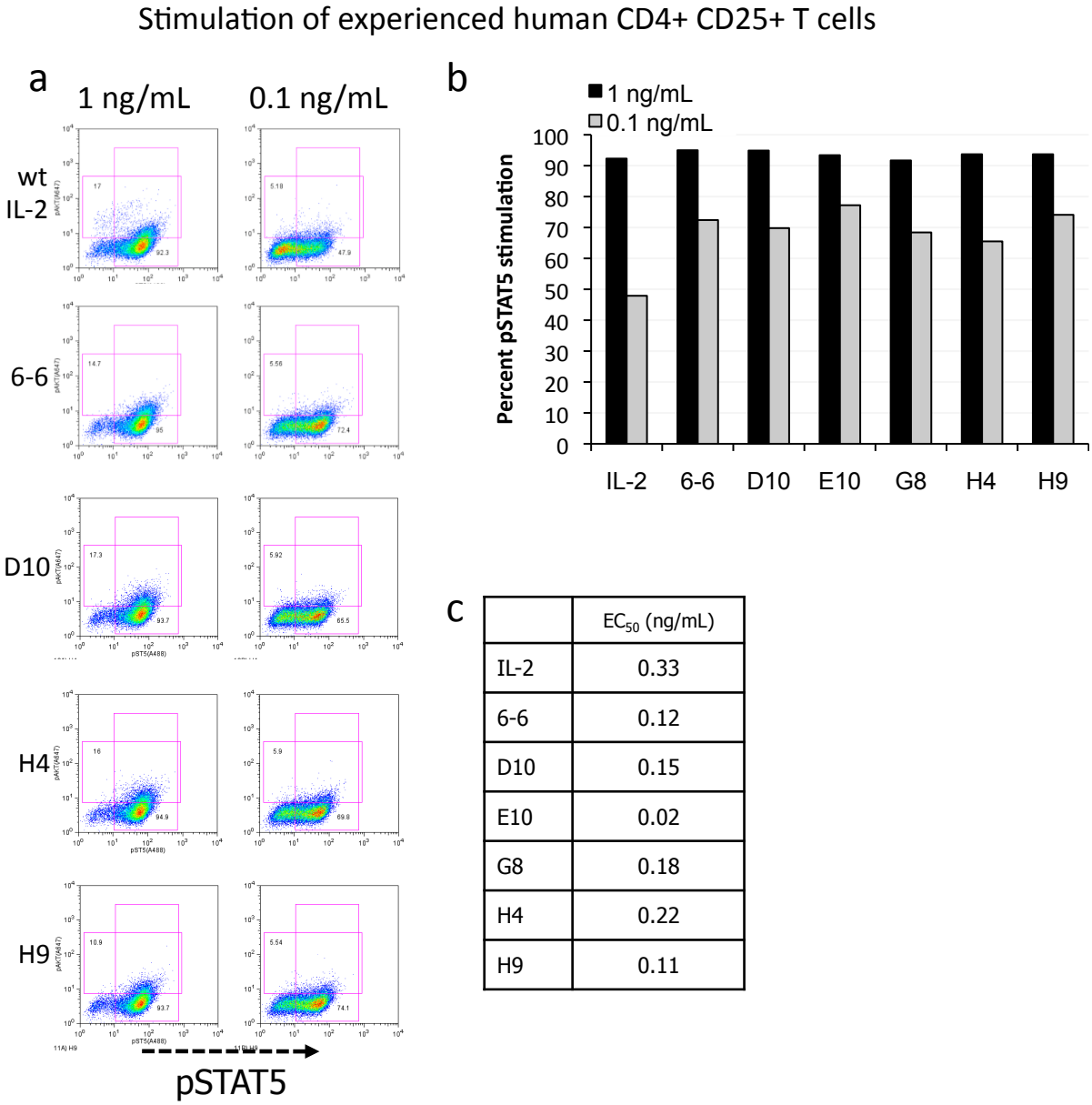

c

	EC_{50} (ng/mL)
IL-2	0.33
6-6	0.12
D10	0.15
E10	0.02
G8	0.18
H4	0.22
H9	0.11

Supplementary Figure 13. Expression of CD25 on experienced human $CD4^+$ T cells negates superkine effect. **a**, Analysis of phosphorylated STAT5 (pSTAT5) on $CD4^+$ $CD25^+$ experienced T cells stimulated with the indicated IL-2 variants. Dose-response curves (**b**) and respective EC_{50} values (**c**) of IL-2 and superkine variant on STAT5 phosphorylation.

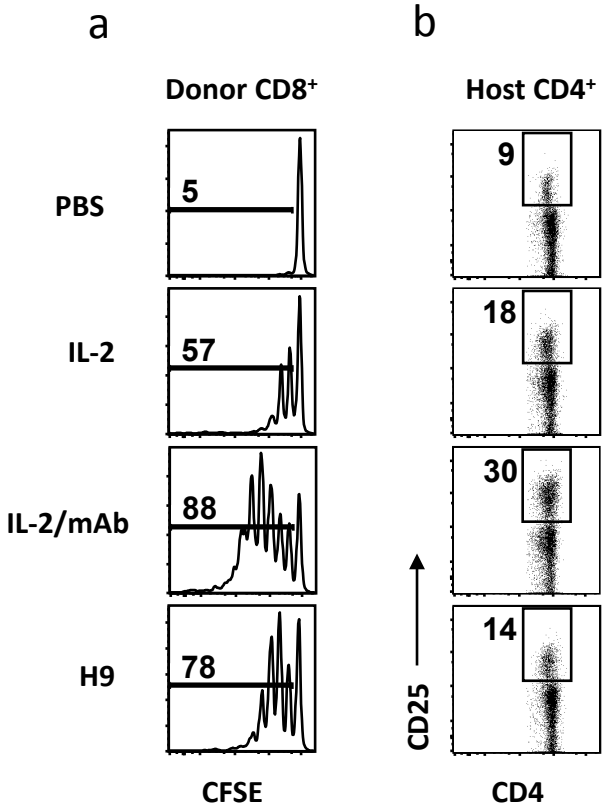

Supplementary Figure 14. *In vivo* T cell expansion. **a**, $CD8^+$ T cells, enriched for memory-phenotype cells expressing high levels of CD44 and IL-2Rβ, were purified from Thy1.1-congenic mice, labeled with the live dye carboxyfluorescein succinimidyl ester (CFSE) in order to monitor cell division, and adoptively transferred to normal Thy1.2-congenic animals. Subsequently, recipient mice were injected daily with either phosphate-buffered saline (PBS, as a control), WT IL-2, IL-2/anti-IL-2 mAb complexes (IL-2/mAb), or H9 super-2 for 5 days, followed by analysis of spleens by flow cytometry. **b**, CD25 expression in host $CD4^+$ T cells from spleens of mice treated as in **a**. See also Fig. 4.

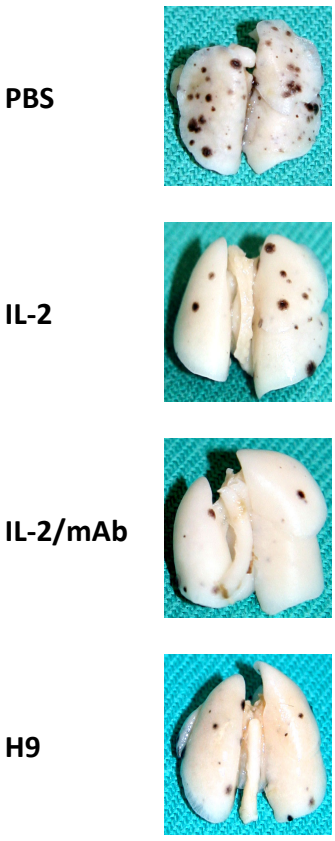

Supplementary Figure 15. Anti-tumor response against pulmonary B16F10 nodules. B6 mice received 3x 10^5 B16F10 cells intravenously, followed by five daily injections of either phosphate-buffered saline (PBS), 20 μg IL-2, 1.5 μg IL-2/anti-IL-2 mAb complexes, or 20 μg H9, starting three days after tumor injection. Shown are photographs of fixed whole lungs on day 16 after tumor injection. See also Fig. 4.

Supplementary Movies :

IL-2_MD.mov
Super-2_MD.mov

Atomistic molecular dynamics simulations of wild-type IL-2 and the D10 mutant show that the mutations in D10 stabilize the B and C helices. In each of these ~50 ns long simulations, the residues that differ between the wild-type and D10 sequences are shown with a sticks representation to highlight their mobility in the wild-type protein relative to D10. These simulations (and the others reported in the manuscript) were run at 300 K with the Gromacs simulation package and visualized with VMD. More details regarding the simulation parameters are also given in the manuscript, and quantitation of the MD results are shown in Figure 3.